Supporting Information

Integrating a Redox-Coupled $FeSe_2$/N-C Photoelectrode into a Potassium Ion Hybrid Capacitors for Photoassisted Charging

Ronghao Wang [a] *Kaiwen Sun* [b] *Hongmin Liu,*[a] *Chengfei Qian,*[a] *Muhan Li,*[a] *Yuhao Zhang,*[a] *Weizhai Bao**[a]

[a]R. Wang, H. Liu, C. Qian, M. Li, Y. Zhang, Prof. W. Bao
School of Chemistry and Materials Science
Nanjing University of Information Science & Technology
Nanjing, 210044, China.
E-mail: weizhai.bao@nuist.edu.cn

[b]Prof. K. Sun
Australian Centre for Advanced Photovoltaics
School of Photovoltaic and Renewable Energy Engineering
University of New South Wales
Sydney, 2052, Australia

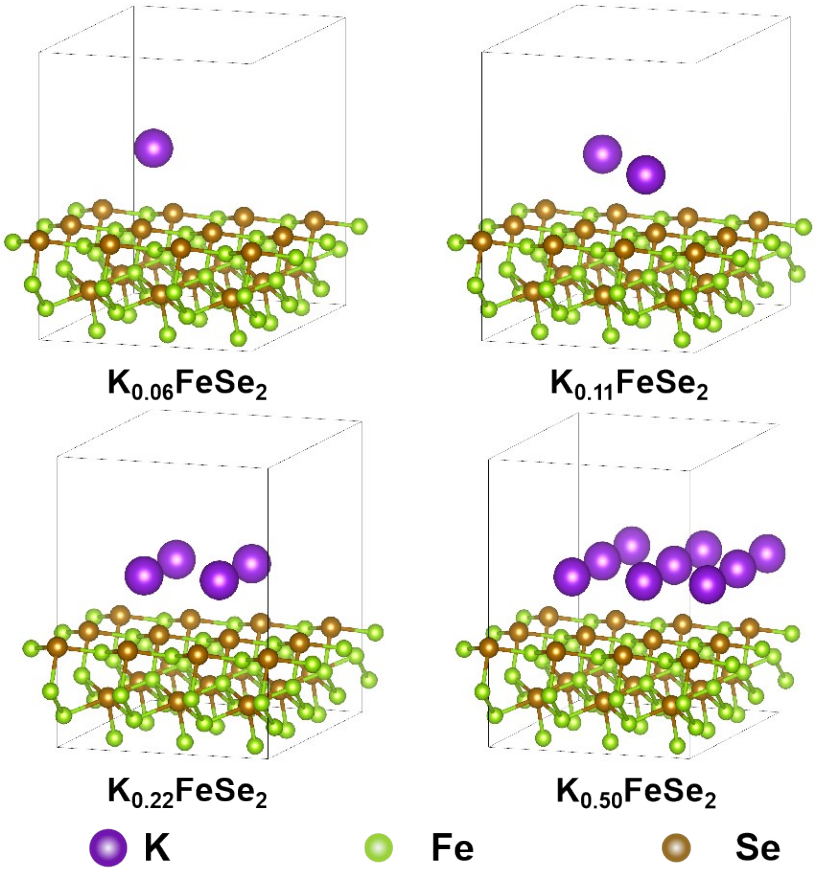

Fig. S1. By calculating the intercalation of different K^+ ratios.

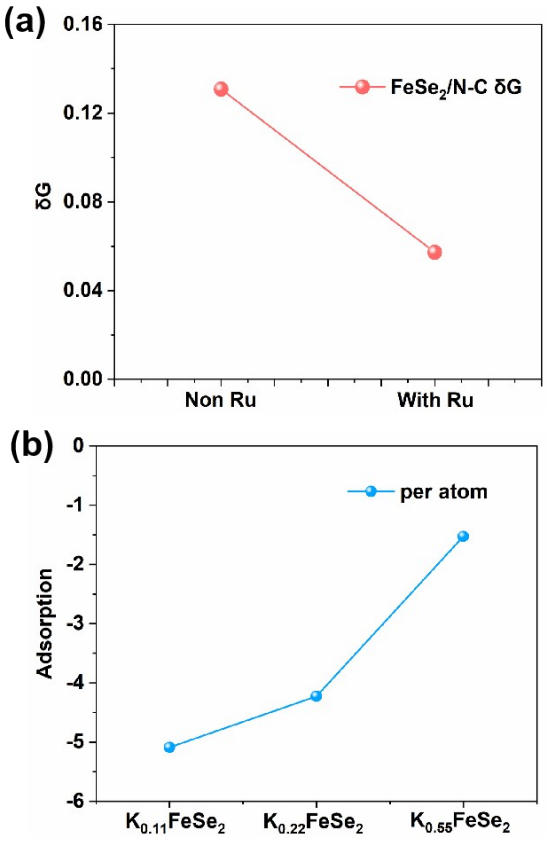

Fig. S2. The data picture of the adsorption energy calculation of K with and without Ru atoms and the data map of the adsorption of potassium in different proportions.

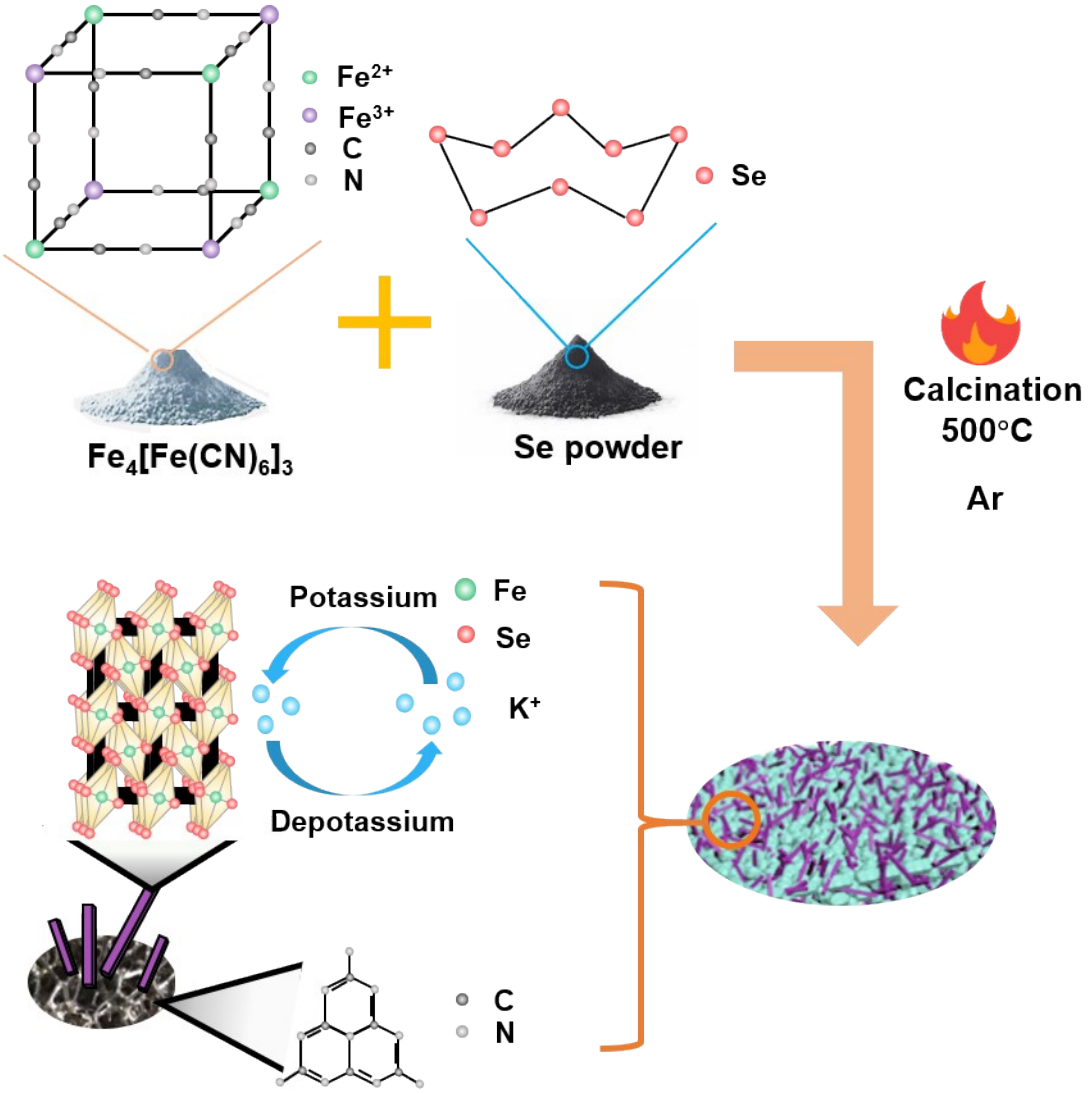

Fig. S3. The schematic diagram of the preparation technology of $FeSe_2$/N-C composites towards promoting the K-storage.

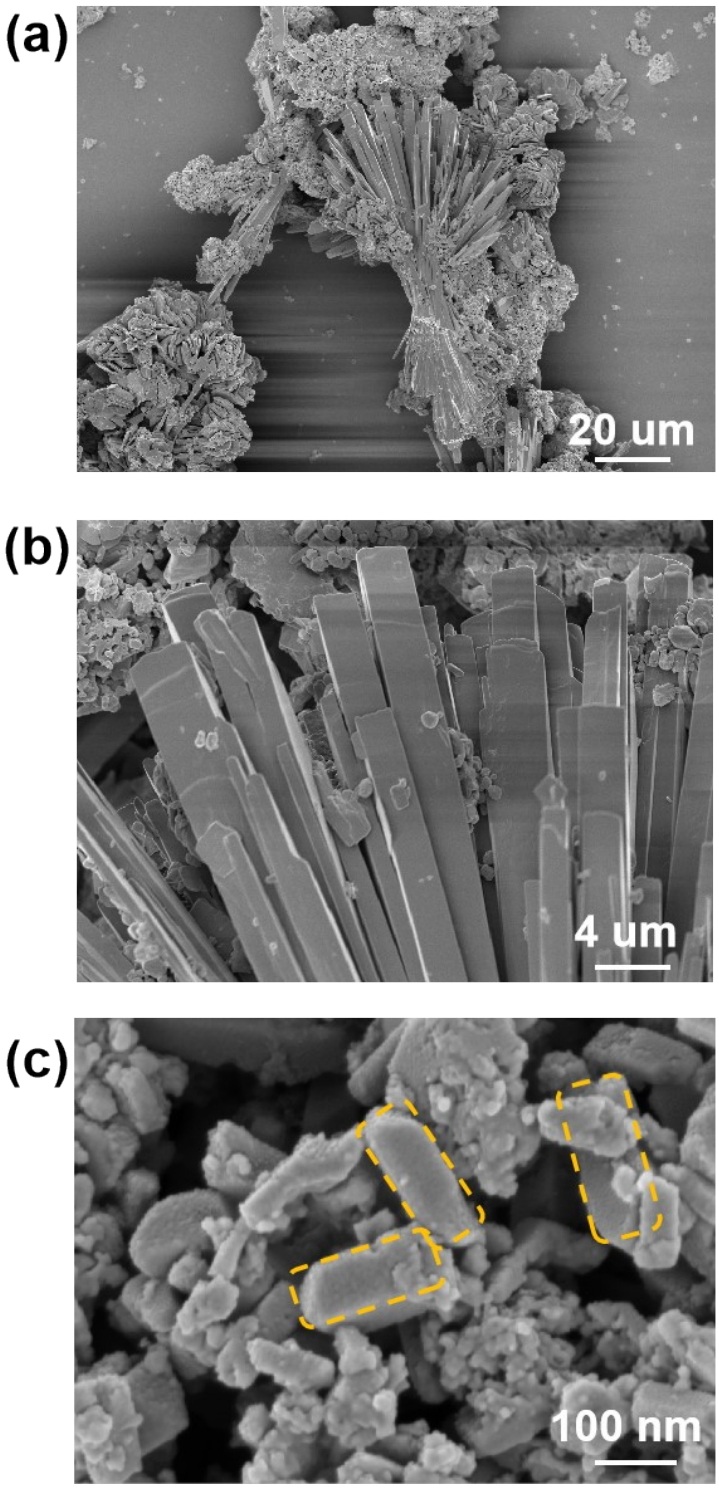

Fig. S4. SEM image of (a, b) the $FeSe_2$ and (c) the $FeSe_2$/N-C

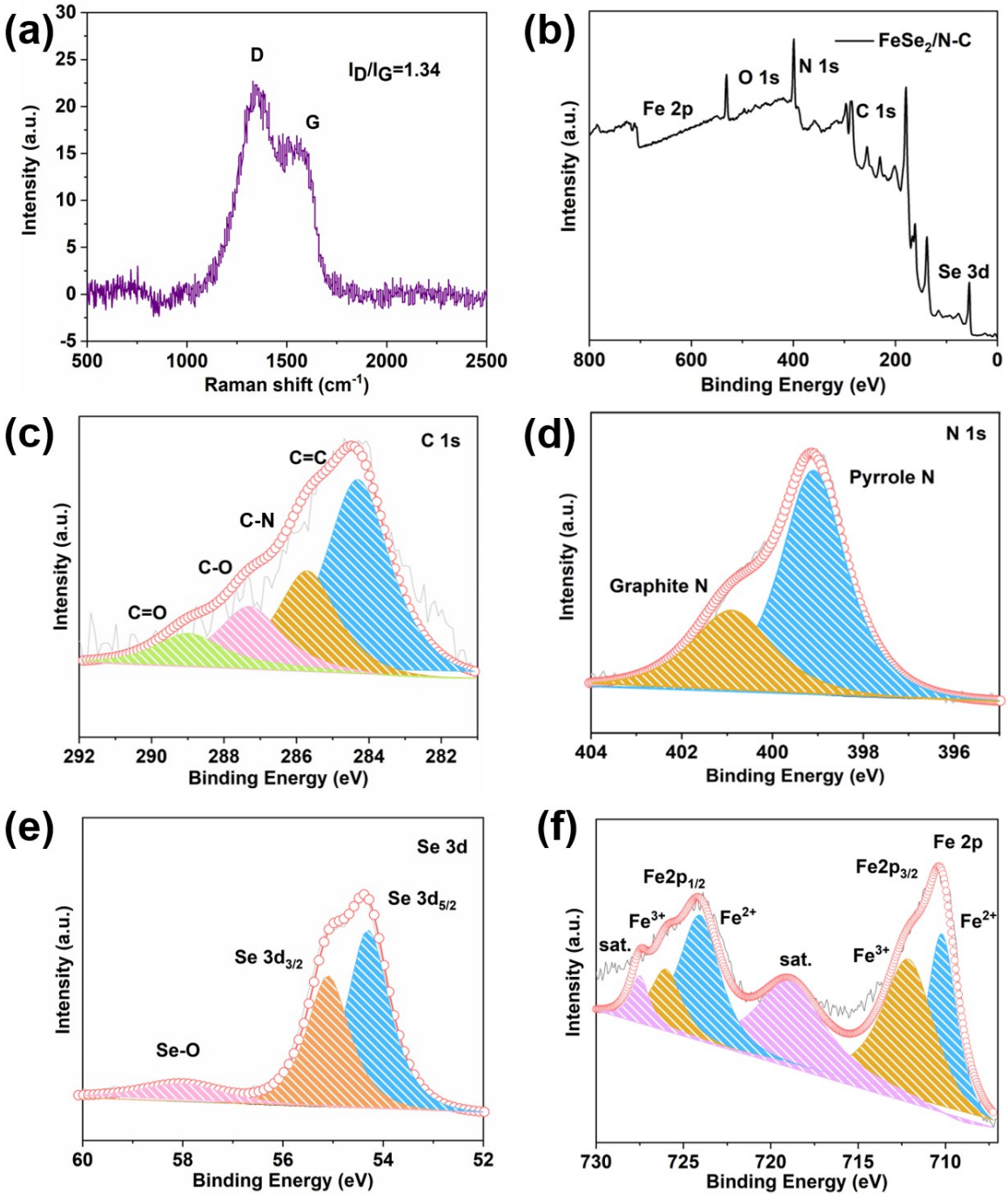

Fig. S5. (a) Raman spectrum and X-ray photoelectronic spectrum (XPS) of the FeSe@N–C structures: (b) survey, (c) C 1s, (d) N 1s, (e) Se 3d, and (f) Fe 2p.

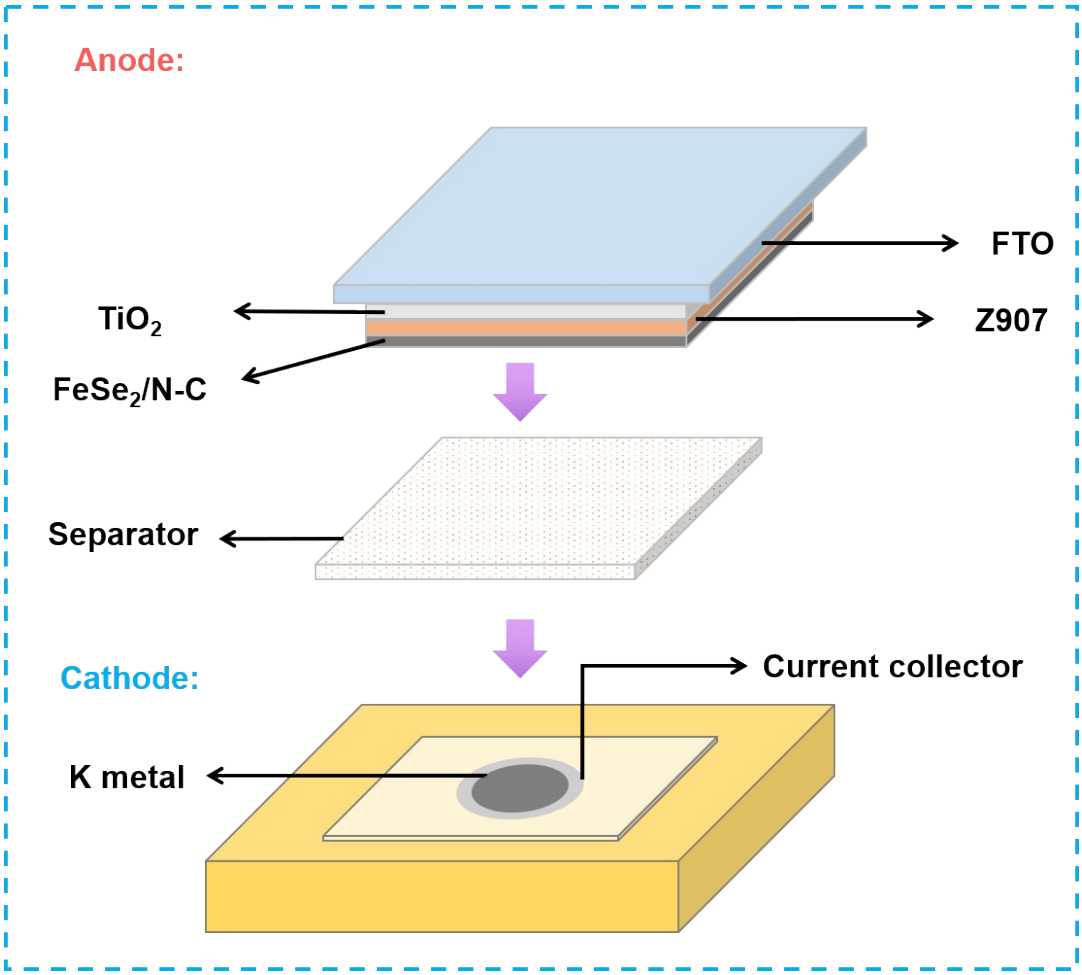

Fig. S6. Schematic of the integrated device (the insert is the corresponding real picture).

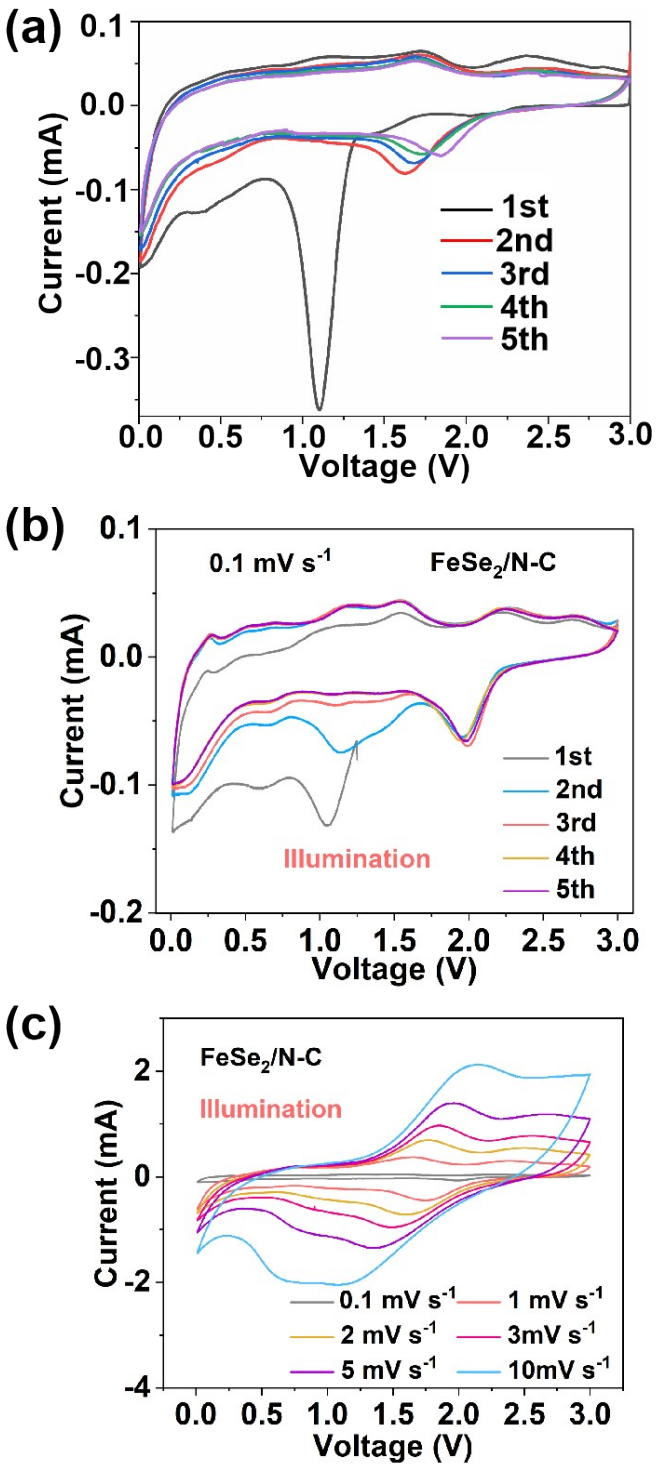

Fig. S7. CV curves of (a) $FeSe_2$ and (b) $FeSe_2$/N-C electrodes at a scan rate of 0.1 mV s^{-1} between 0.01 and 3 V (vs. K^+/K). (c) CV curves of the $FeSe_2$/N-C at different scan rates.

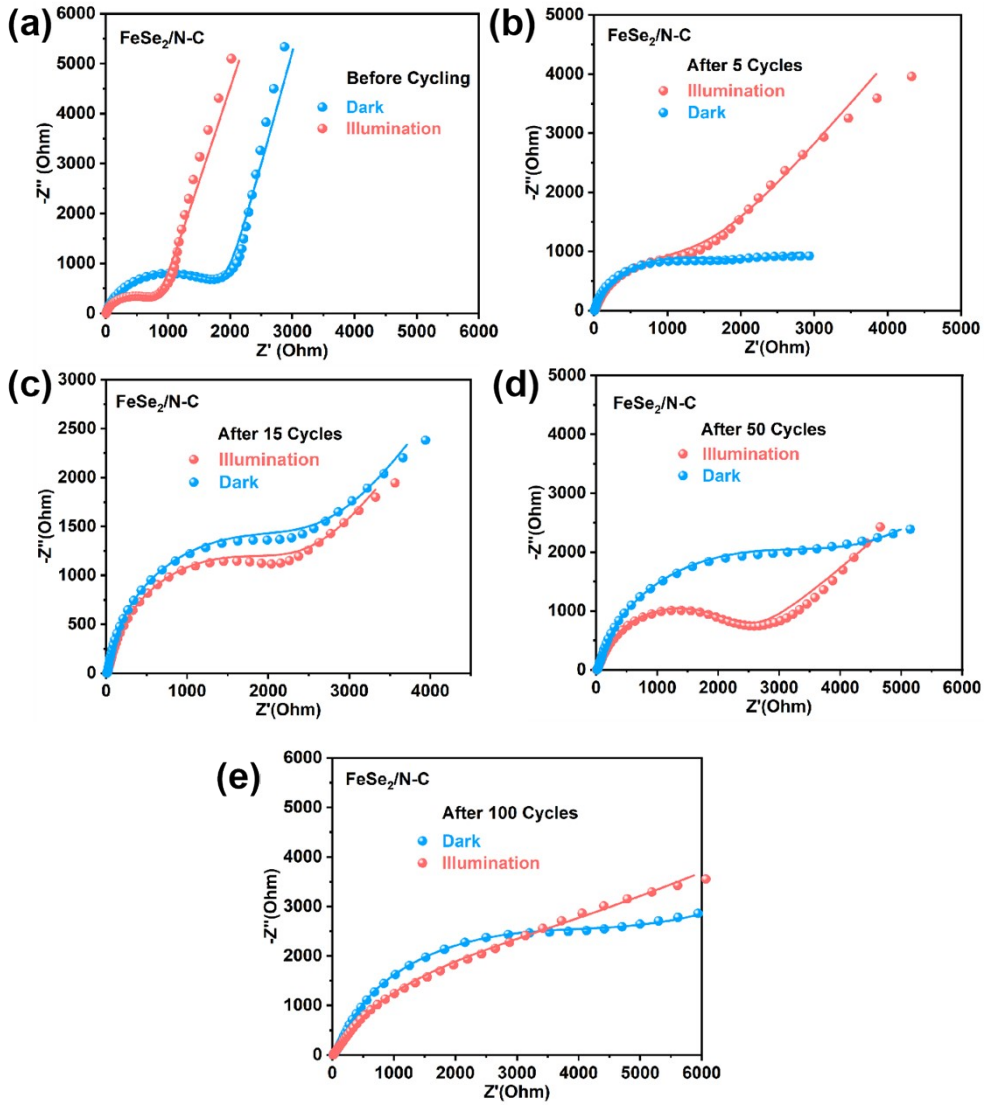

Fig. S8. (a-e) EIS for before cycle, 5h, 15th, 50th and 100th cycles.

In the dark: The delta values for the fifth cycle before cycling and after cycling show an increase, which is attributed to the formation of the SEI film. Second, the delta value gradually increases in the subsequent cycles. This is attributed to the generation of irreversible products and the gradual reduction of electrolyte during normal battery cycling.

In the illumination: This is due to the kinetic enhancement of K^+ promoted by the light effect of the integrated electrode under illumination. In the fifth and fiftieth circles, there is a significant decrease in the phenomenon, which may be due to the alternating on and off of the light, and the temperature increases slightly during the light. However, in general, the δ value showed a gradual decrease before and after cycling, which also indicated the positive effect of the light effect.

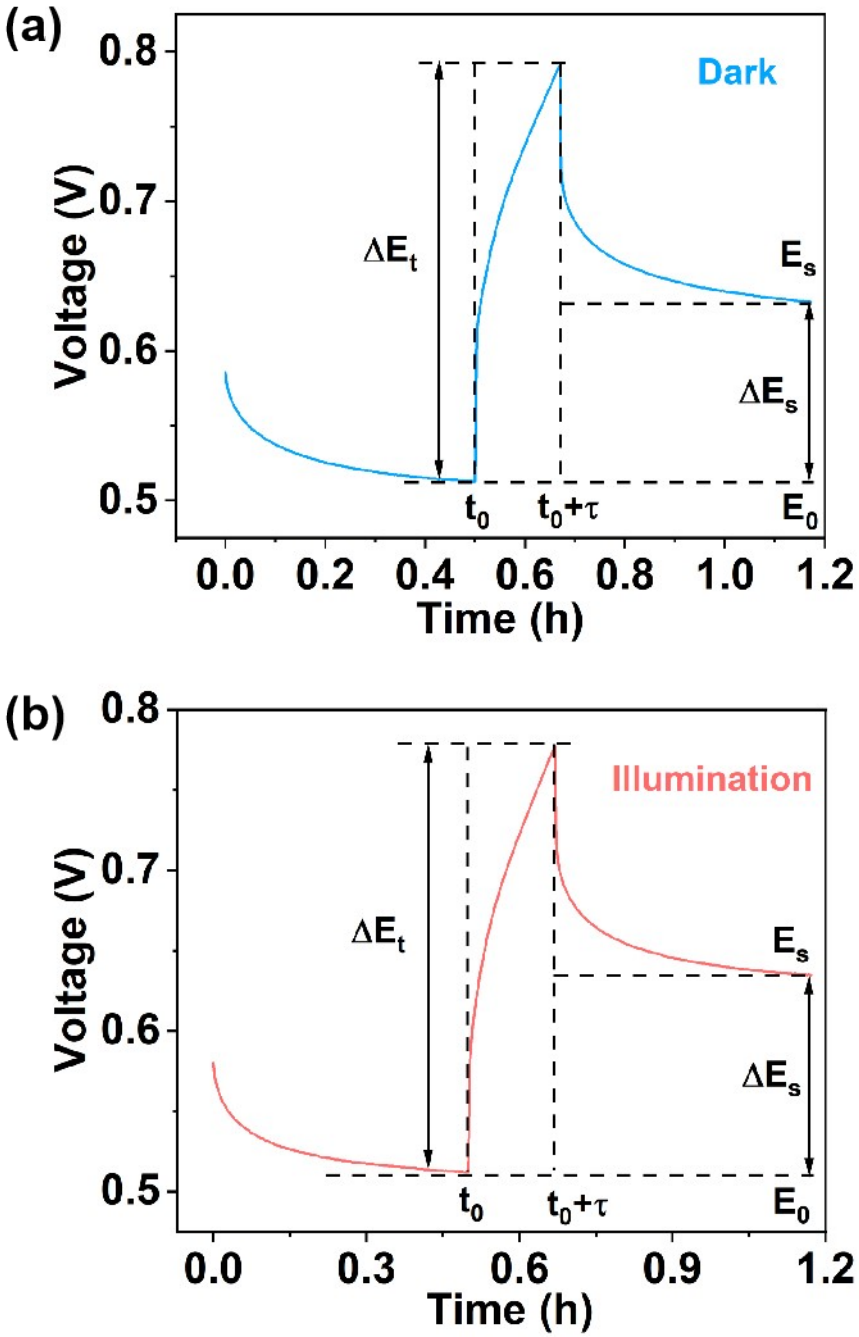

Fig. S9. Current step diagram of (a) dark and (b) illunination at 0.6 V versus K^+/K in the first depotassiation process.

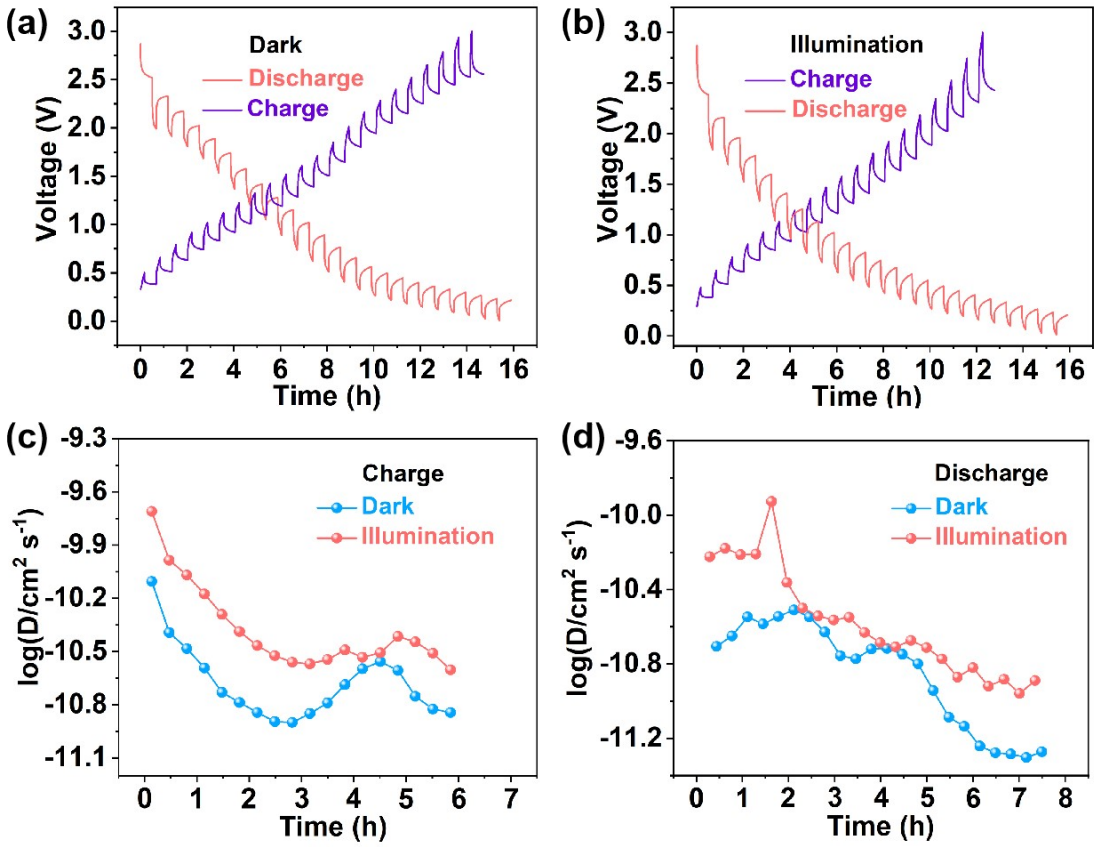

Fig. S10. Galvanostatic intermittent titration technique results for $FeSe_2$/N-C in (a) dark and (b) illumination conditions measured at 100 mA g^{-1}. The variation of diffusion coefficients for $FeSe_2$/N-C in dark and illumination conditions upon (c) potassiation and (d) depotassiation.

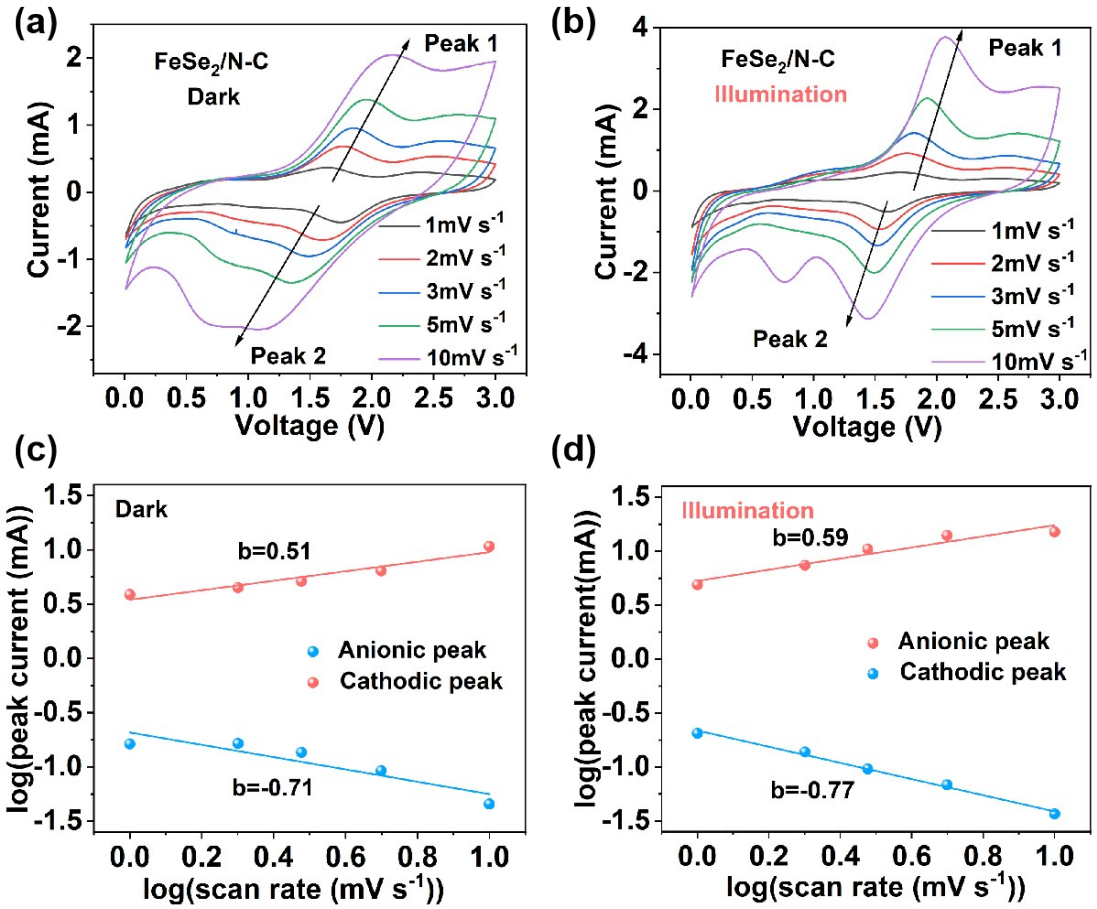

Fig. S11. The CV curves at stepwise scan rates (1, 2, 3, 5, and 10 mV s^{-1}) for $FeSe_2$/N-C in (a) dark and (b) illumination conditions. b-value analysis using the relationship between the peak currents and scan rates for $FeSe_2$/N-C in (c) dark and (d) illumination conditions.

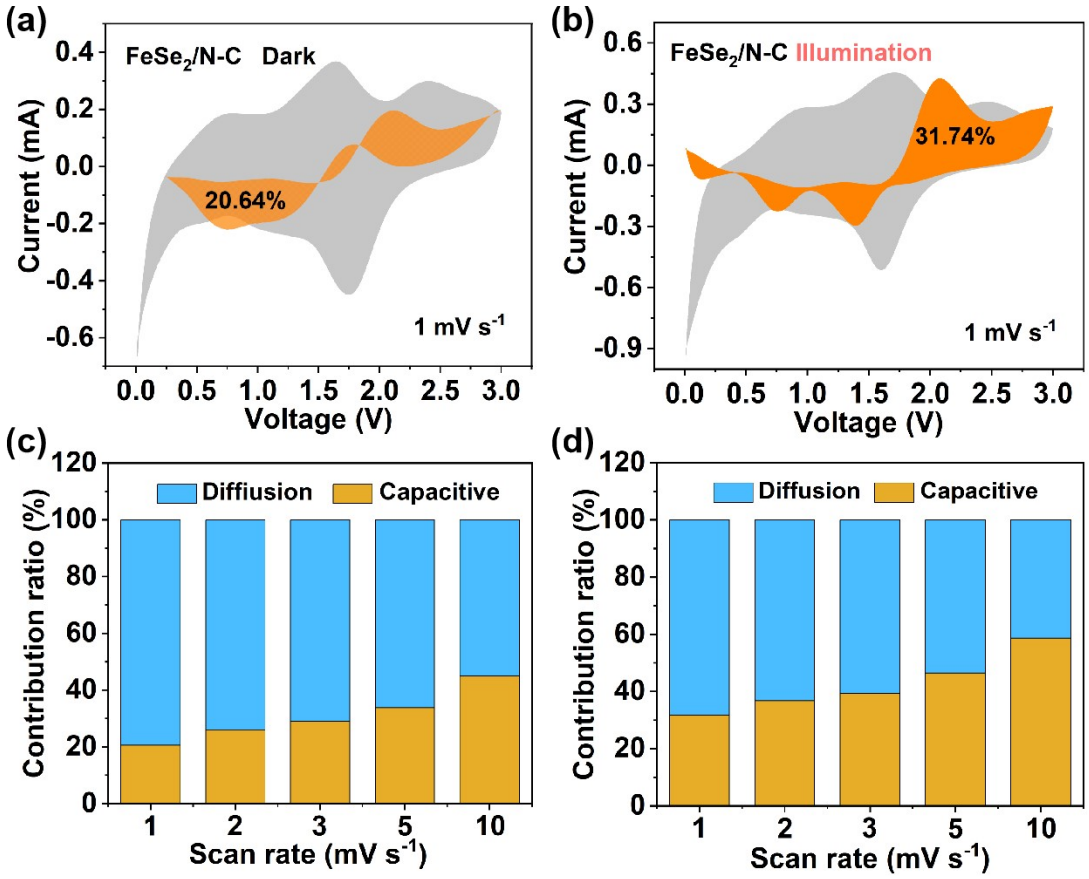

Fig. S12. CV curves and surface-controlled capacitive contributions of $FeSe_2$/N-C in (a) dark and (b) illumination conditions shown in the orange regions (1 mV s^{-1}). The capacitive contribution histograms of $FeSe_2$/N-C in (c) dark and (d) illumination conditions at scan rates from 1 to 10 mV s^{-1}.

The CV integral area under light is larger and slightly distorted, while the CV integral area under dark conditions is smaller and severely distorted. The reason for this better capacitance may be that the photoelectric effect promotes the surface diffusion of K^+ under illumination conditions, which increases the rate of ion diffusion. At a scan rate of 10 mV s^{-1}, the surface capacitance contribution is about 58.7 % of the total charge storage, which is much larger than that of diffusion control, indicating that the $FeSe_2$/N-C integrated photoelectrode has an efficient surface charge storage capability.

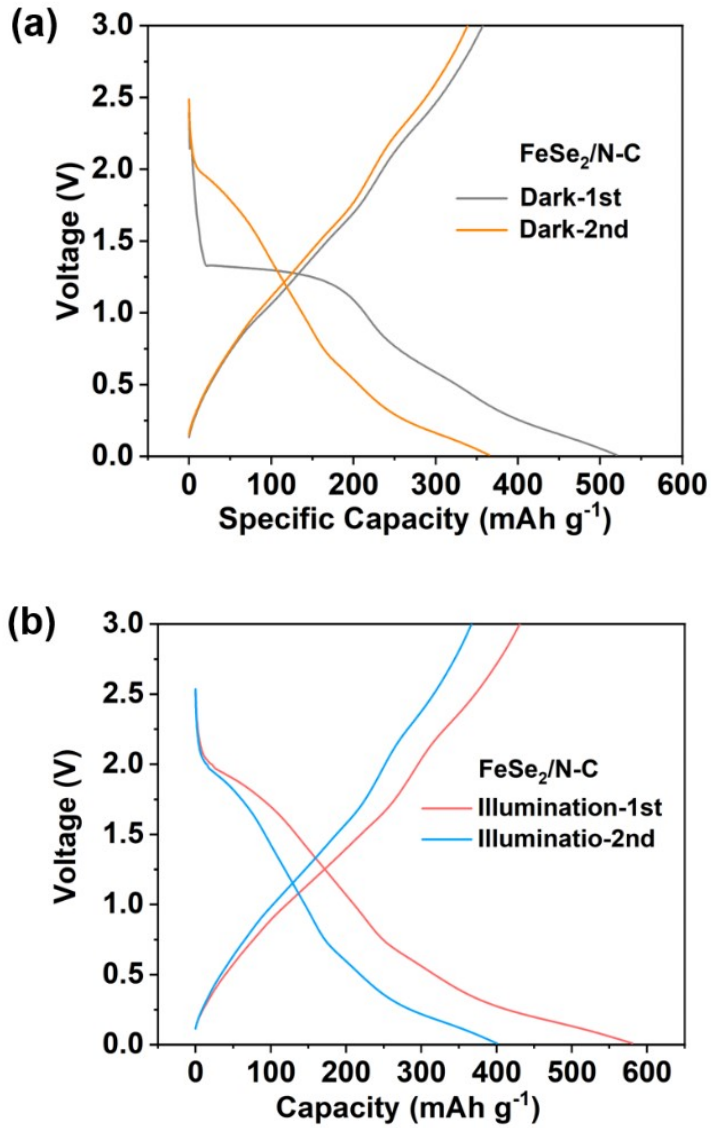

Fig. S13 The charge-discharge profiles of battery with the dark and the illuminatio at 100 mA g^{-1}. The initial Coulombic efficiencies with and without light were 74.5 % and 66.3 %, respectively, and the larger initial irreversible capacity was mainly due to the formation of SEI. Combined with the semicircle in the high frequency region in the impedance (**Fig. S8**), the semicircle is smaller in the case of illumination, which is attributed to the formation of SEI.

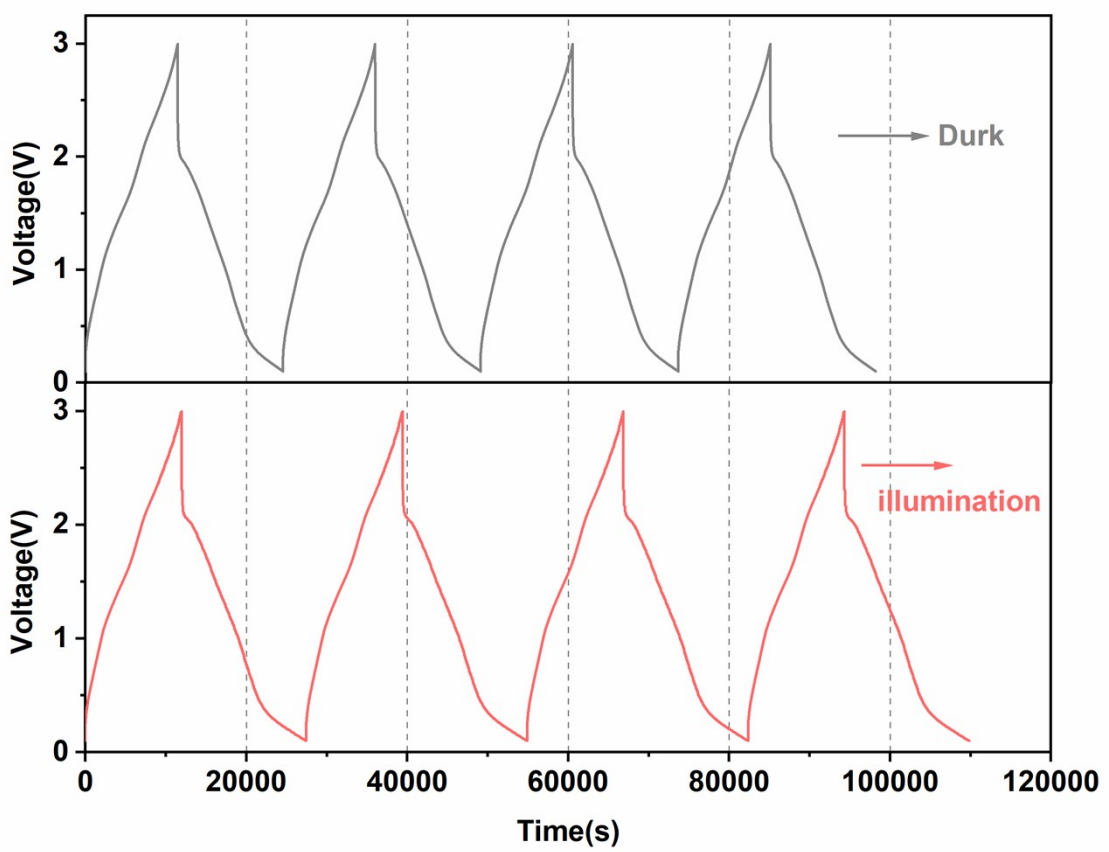

Fig. S14. Galvanostatic charge-discharge profiles at 0.1 A g^{-1} under dark condition (black line) and light illumination (red line).

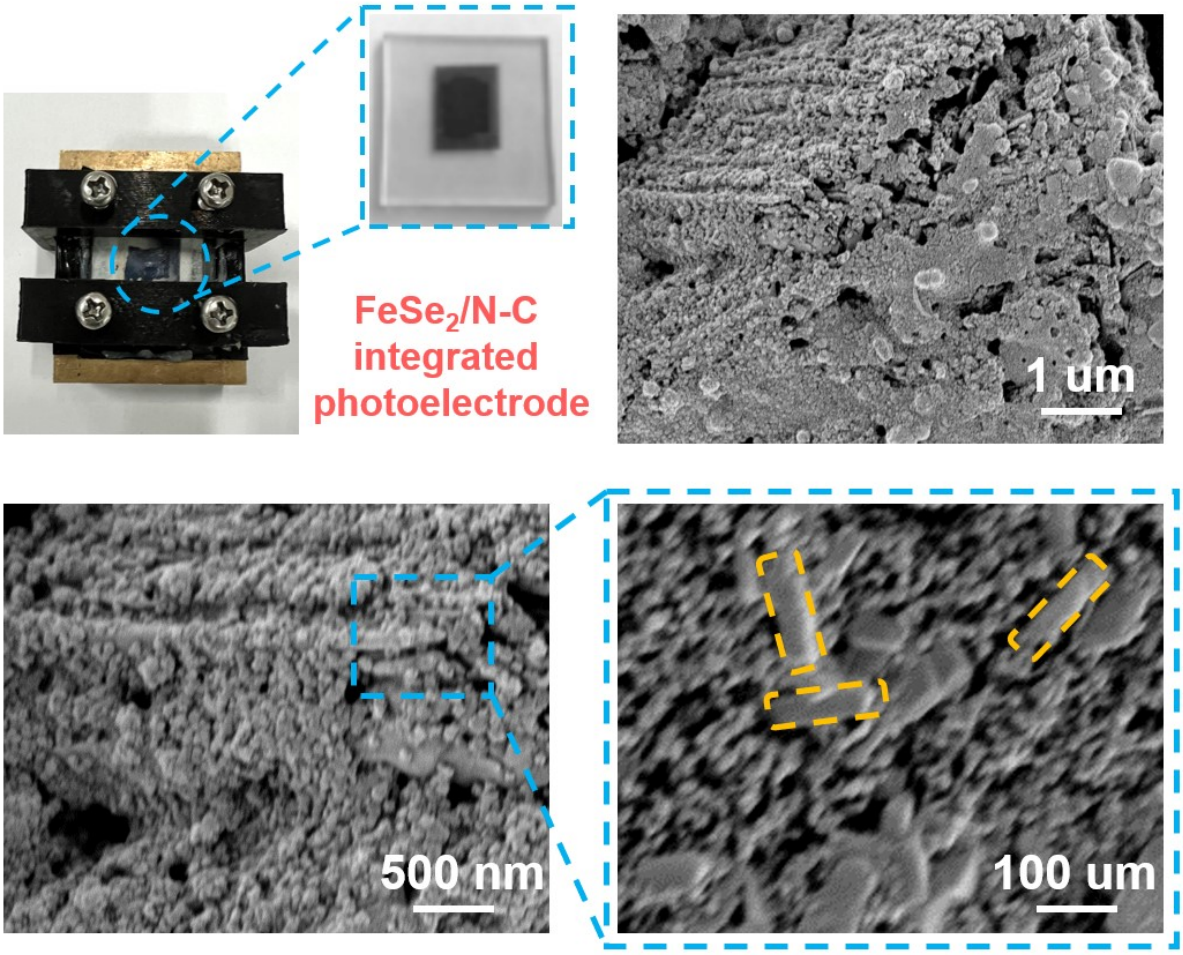

Fig. S15 Microstructure of FeSe2/N-C photoelectrode after 100 cycles under illumination.

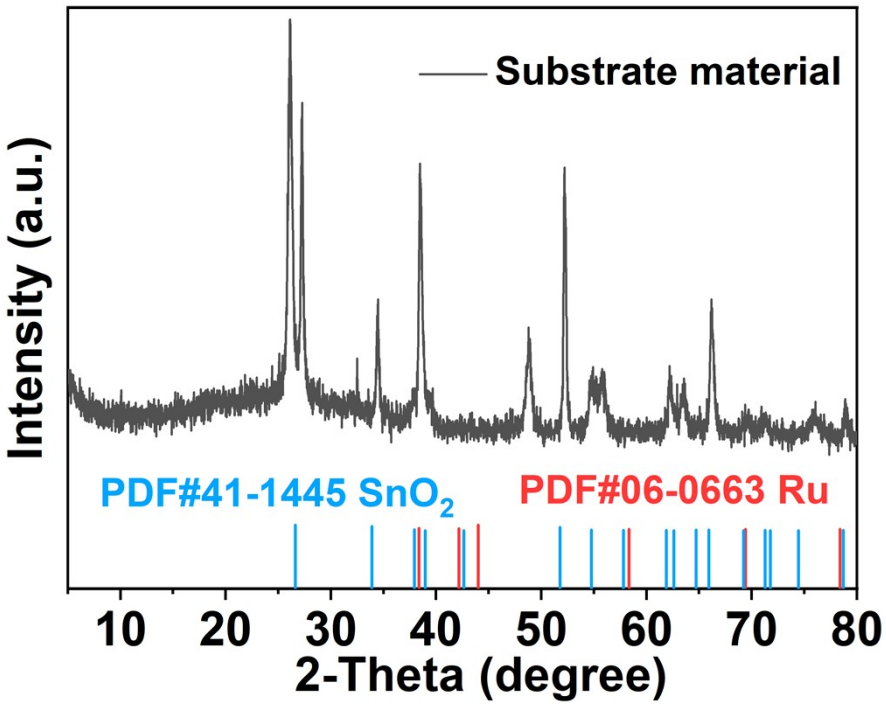

Fig. S16. XRD pattern of the substrate material.

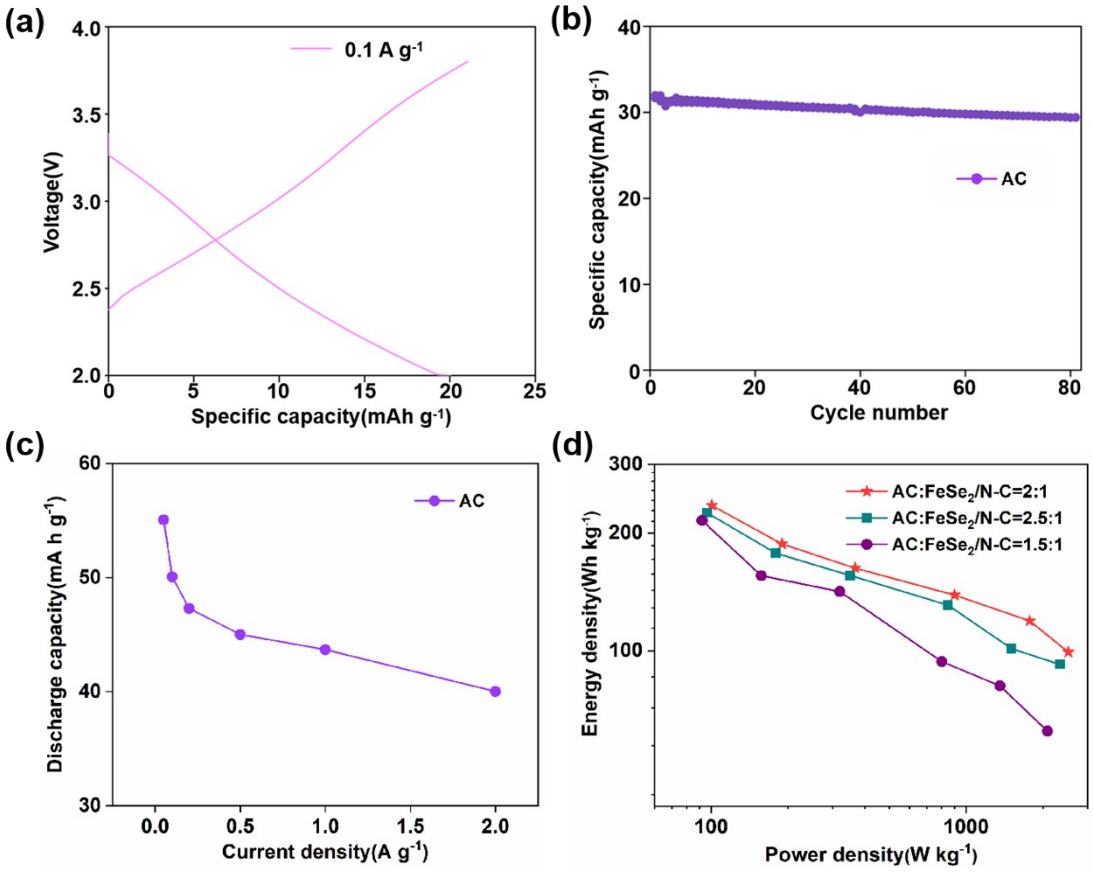

Fig. S17. Electrochemical performances of the AC cathode in K-half cells. (a) Galvanostatic charge and discharge voltage profiles of the AC cathode within the potential range from 2.0 to 3.8 V (vs. K^+/K) at a current density of 0.1 A g^{-1}. (b) Cycling performance of the AC cathode at a current density of 0.1 A g^{-1} for 100 cycles. (c) Rate performance of the AC cathode at various current densities. (d) Ragone plots of $FeSe_2$/N-C//AC with different mass ratios of anode to cathode.

Selecting the mass-to-load ratio of cathodes and anodes: Before assembling PA-PIHCs, we systematically investigated the electrochemical properties of ACs, including charge-discharge curves, cycling and rate performance (**Fig. S17**), showing good electrochemical performance as cathodes for PA-PIHCs . By matching different mass ratios of positive and negative cathode electrodes, the optimal mass ratio of 1:2 (between anode and anode) was selected to achieve the maximum output power (**Fig. S17**).

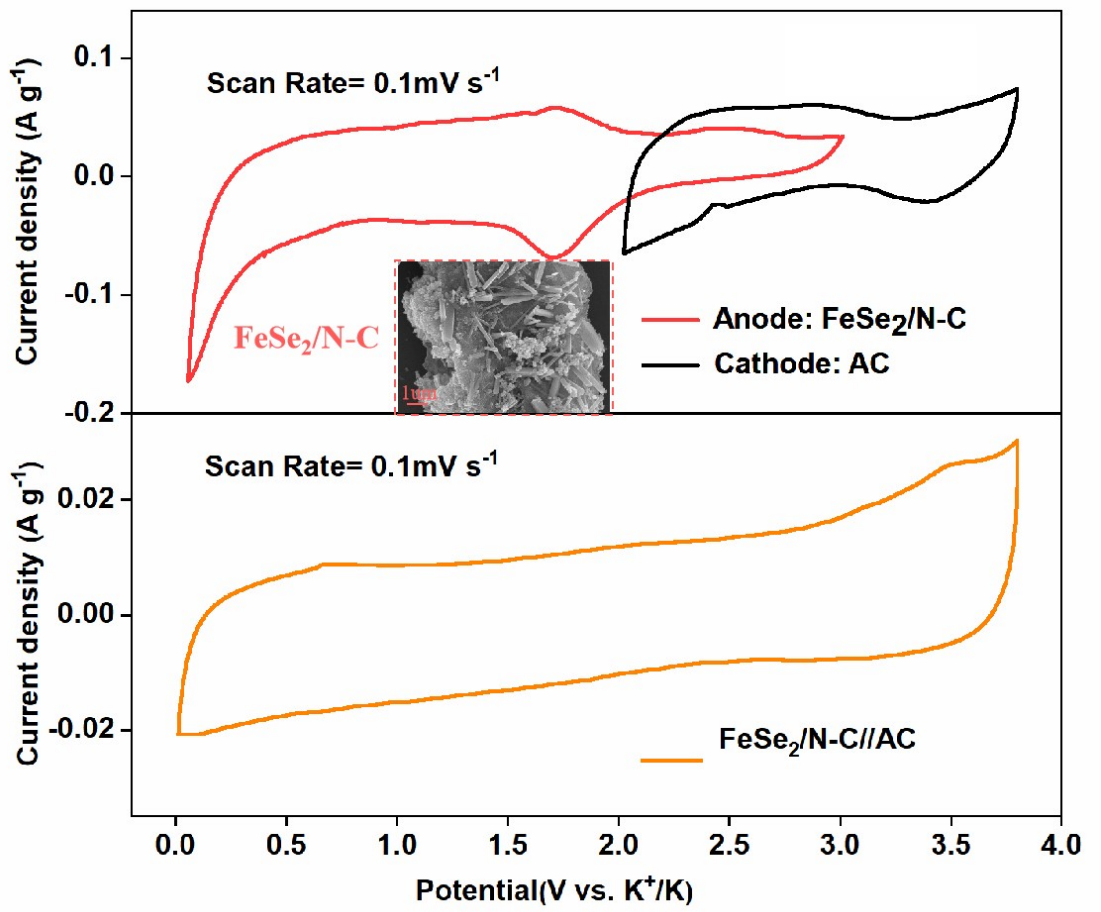

Fig. S18. CV curves of the $FeSe_2$/N-C anode and the AC cathode in half cells (top) and PIHCs (bottom) at 0.1 mV s^{-1}.

Setting of the voltage window: According to the CV curve of the positive and negative materials, the voltage window of the PA-PHIC is finally obtained by comparing the curve shape and area. **Fig. S18** demonstrates that the assembled PIHCs are electrochemically stable at a given voltage range (0.01 to 3.8 V).

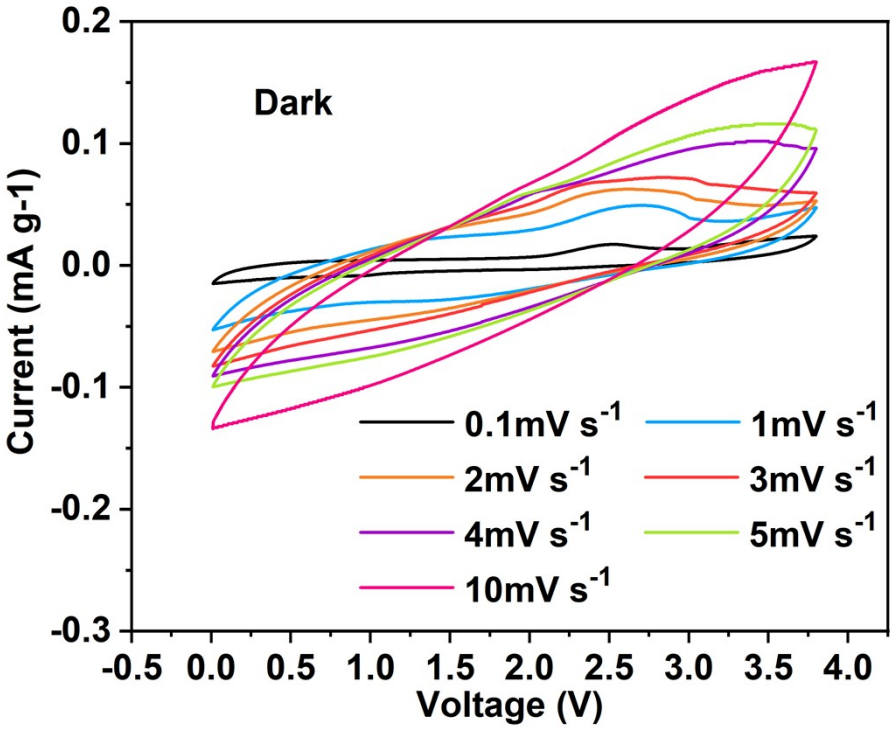

Fig. S19. CV curves of the $FeSe_2$/N-C//AC at different scan rates.

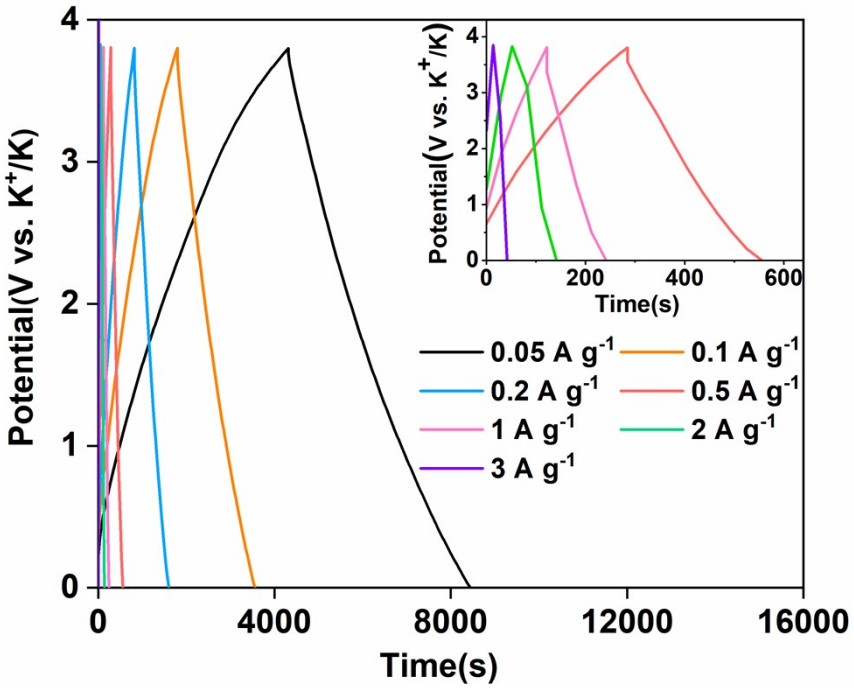

Fig. S20. $FeSe_2$/N-C//AC PIHC's GCD curve corresponding to different current densities under different conditions in dulk.

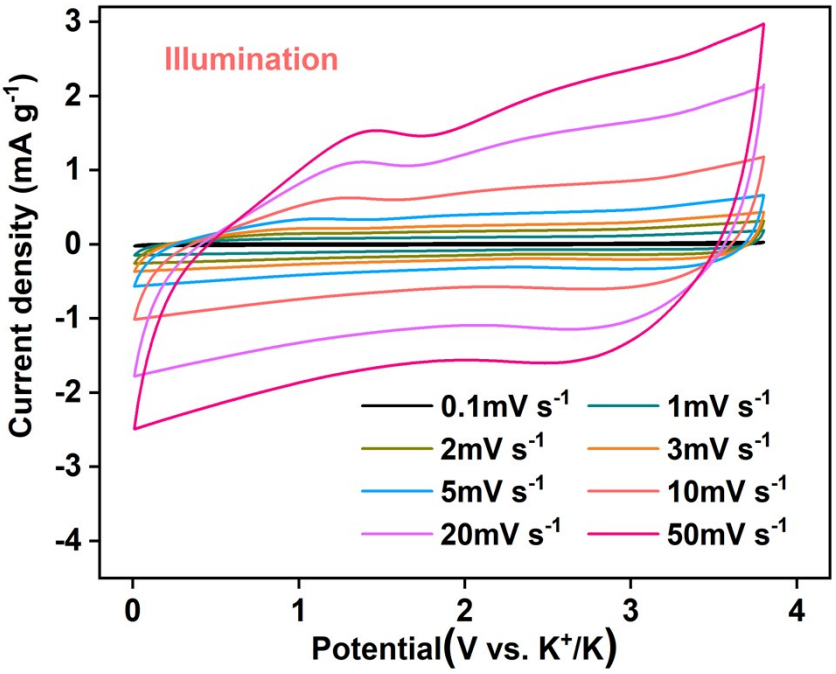

Fig. S21. CV curves of the $FeSe_2$/N-C//AC at different scan rates.

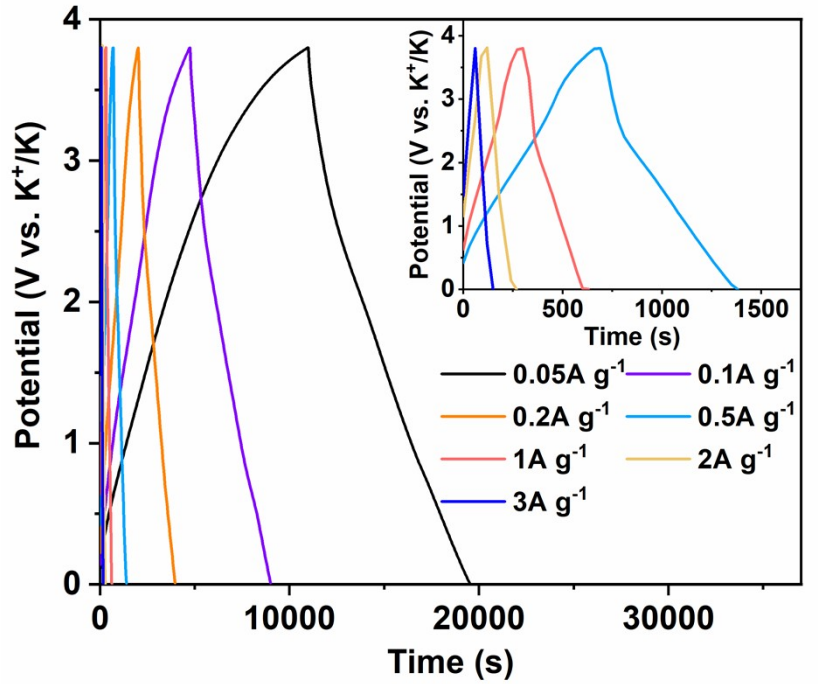

Fig. S22. PA-PIHC's GCD curve corresponding to different current densities under different conditions in illumination.

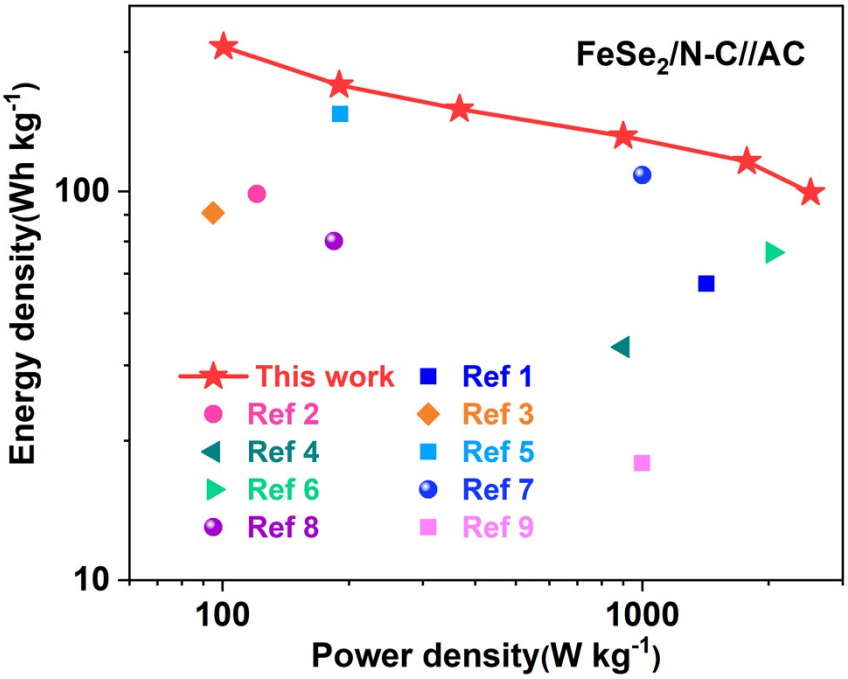

Fig. S23. Ragone plots of different hybrid capacitors according to previous works.

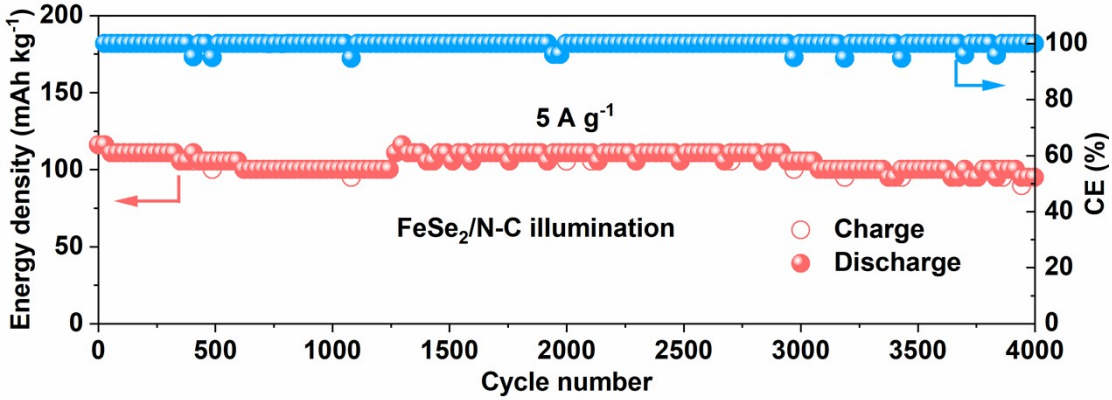

Fig. S24. Long-term cycle performance of the PA-PIHC device at 5 A g^{-1} light illumination up to 4000 cycles.

Reference:

1. X. Liu, G. A. Elia, B. Qin, H. Zhang, P. Ruschhaupt, S. Fang, A. Varzi and S. Passerini, *ACS Energy Lett.*, 2019, **4**, 2675-2682.

2. Y.-Z. Fang, R. Hu, K. Zhu, K. Ye, J. Yan, G. Wang and D. Cao, *Adv. Funct. Mater.*, 2020, **30**, 2005663.

3. J. Dong, Y. He, Y. Jiang, S. Tan, Q. Wei, F. Xiong, Z. Chu, Q. An and L. Mai, *Nano Energy*, 2020, **73**, 104838.

4. H. Peng, B. Yao, X. Wei, T. Liu, T. Kou, P. Xiao, Y. Zhang and Y. Li, *Adv. Energy Mater.*, 2019, **9**, 1803665.

5. J. Ruan, F. Mo, Z. Chen, M. Liu, S. Zheng, R. Wu, F. Fang, Y. Song and D. Sun, *Adv. Energy Mater.*, 2020, **10**, 1904045.

6. W. Zong, N. Chui, Z. Tian, Y. Li, C. Yang, D. Rao, W. Wang, J. Huang, J. Wang, F. Lai and T. Liu, *Adv. Sci.*, 2021, **8**, 2004142.

7. Y. Peng, R. Zhang, B. Fan, W. Li, Z. Chen, H. Liu, P. Gao, S. Ni, J. Liu and X. Chen, *Small*, 2020, **16**, 2003724.

8. W. Li, R. Zhang, Z. Chen, B. Fan, K. Xiao, H. Liu, P. Gao, J. Wu, C. Tu and J. Liu, *Small*, 2021, **17**, 2100397.

9. H. V. Ramasamy, B. Senthilkumar, P. Barpanda and Y.-S. Lee, *Chem. Eng. J.*, 2019, **368**, 235-243.